Final report

1. Project details

Project title	EUDP17-II: IEA PVPS Task 16 Solar ressource for high penetration (2017-20)
File no.	64017-05163
Name of the funding scheme	EUDP
Project managing company / institution	DTU Byg, Danmarks Tekniske Universitet
CVR number (central business register)	30060946
Project partners	
Submission date	4/12-2020

Authors: Simon Furbo (DTU), Elsabet Nielsen (DTU), Kristian Pagh Nielsen (DMI), Adam R. Jensen (DTU)

2. Summary

The purpose of the project was to achieve a better understanding of the solar energy resource, so that better recommendations on energy systems with high degree of renewable energy penetration can be given. This was done as an international collaboration within the IEA PVPS programme by participation in the IEA Task 16 project Solar resource for high penetration.

A detailed simulation model to determine the solar radiation on panels and the performance of solar collectors and photovoltaic (PV) panels installed in large fields was developed. Different distances between the panel rows and different panel tilts was investigated. The model was validated by detailed measurements from a laboratory test facility with two rows of solar collectors with a variable row distance and variable collector tilt. Furthermore, the diffuse solar radiation from different parts of the sky was elucidated by means of measurements from the climate station of the Technical University of Denmark. The analyses showed that the diffuse radiation from the sky is much higher from the region close to the Sun disc than from the other parts of the sky under sunny conditions. Under cloudy conditions the diffuse radiation can be considered as isotropic. Additionally, the long-term variability of solar radiation was elucidated. The influence of the variable yearly solar radiation on the yearly thermal performances of Danish solar heating plants was elucidated by means of measurements and calculations. It was found that approximately half of the yearly variations of the thermal performances experienced is caused by variations of solar radiation from year to year and from location to location.

Formålet med projektet var at opnå en bedre forståelse af solenergi-ressourcerne, så der kan gives bedre anbefalinger for anvendelse af energisystemer med en høj grad af integrering af vedvarende energi. Dette blev gjort som en del af det internationale IEA PVPS samarbejdsprogram ved deltagelse i IEA Task 16 projektet Solar ressource for high penetration.

En detaljeret simuleringsmodel til bestemmelse af solstråling på og ydelse af solfangere og PV paneler opstillet i store felter blev udviklet. Forskellige afstande mellem solpanelrækkerne og forskellige solpanelhældningerne blev undersøgt. Simuleringsmodellen blev valideret ved hjælp af målinger fra en laboratorieopstilling med to solfangerrækker med variabel rækkeafstand and med variabel solfangerhældning. Desuden blev det ved hjælp af målinger fra klimastationen på Danmarks Tekniske Universitet klarlagt fra hvilke dele af himmelen den diffuse solstråling stammer. Analyserne viste at den største del af den diffuse solstråling i solrige perioder stammer fra den del af himmelen, der er nærmest solskiven, og at den diffuse stråling er isotrop i overskyet vejr. Solstrålingens variabilitet på lang sigt blev klarlagt. Desuden blev det ved hjælp af målinger og beregninger klarlagt, hvorledes de årlige forskelle i solstråling påvirker danske solvarmecentralers årlige ydelser. Omtrent halvdelen af forskellene mellem de årlige ydelser for solvarmecentralerne er forårsaget af årlige forskelle i solstråling fra år til år og fra lokalitet til lokalitet.

3. Project objectives

The objectives of the project were, through participation in the international IEA Task 16 project *Solar resource for high penetration,* to achieve a better understanding of the solar energy resource and to develop a simulation model capable of modelling the non-uniform distribution of solar radiation on solar collectors/PV panels and the performance of the solar collectors/PV panels in large solar fields. Furthermore, the project aimed to elucidate the long-term variability of the solar resource, and reduce the uncertainty of solar radiation data by developing new quality control procedures.

The project had the following work packages (WPs) and milestones:

WP1 – Project management. Meetings were arranged with DMI to coordinate the project activities.

WP2 – Evaluation of resource assessment products & quality-control. This WP corresponded to Subtask 1 in the international task work. Investigations on solar radiation and performance of solar collectors/PV panels in differently designed solar fields were carried out. The first project milestone, measurements of solar radiation in a laboratory solar collector field, was achieved as planned.

WP3 – Enhanced solar resource assessment. This WP corresponded to Subtask 2 in the international task work. The project contributed with activities in four fields of the IEA Task 16 project: Data quality & formatting, inter-hourly and hourly spatio-temporal variability of the solar resource, long-term inter-annual variability and products for end-users.

The second milestone of the project was achieved by means of the guide “Recommendations on good practices for the preprocessing, quality control of solar radiation measurements and example of validation tools” worked out together with the international partners of the IEA Task project.

WP4 – Travels & Meetings. All the international task meetings, both the physical meetings and the online meetings were attended. Further, a number of relevant conferences and meetings were attended.

WP5 – Dissemination of results. The results were presented at the IEA Task 16 experts meetings and at external meetings and conferences, by contributions to the IEA Task 16 homepage and by a report jointly

prepared by participants of the IEA Task project. Also, the project results have been disseminated in two scientific papers. The third milestone of the project was achieved by the final project report.

The project was carried out as originally planned and all the milestones agreed upon were achieved. The risk that poor weather would make the measurements of solar radiation difficult, was not experienced.

4. Project implementation

The project was executed according to the original plan, with participation in all of the activities mentioned in the project description and delivery of the specified milestones. The project was only slightly affected by the covid-19 pandemic, primarily that the two experts meetings in 2020 were held virtually instead of in person.

The main risk of the project was the possibility of poor weather, which potentially could have resulted in insufficient measurements and an extension of the measurement campaign period. It was also for this reason that the measurement campaign was started at the very beginning of the project, in order to have time at the end of the project in case additional measurements would have to be made. The weather during the project period was overall favourable and the entire measurement campaign was carried out according to the plan.

5. Project results

The main objective of the project was to increase the understanding of the solar resource and enhance the state-of-the-art by developing an accurate model to take into account the non-uniform distribution of radiation in solar fields for enhanced prediction of power output. An overview of the results from the measurement campaign is described in section 5.1 and the model development and validation is described in section 5.2. The full details of these results are published in a scientific article (Tscopp et al., 2020). Enhanced procedures for quality control of solar radiation data were also investigated, presented in section 5.3.

Analyses of diffuse radiation measurements and investigations on long-term inter-annual variability of solar radiation are presented in section 5.4 and 5.5. An overview of products for end-users and investigations on how the variation of yearly solar radiation influence the yearly thermal performance of solar heating plants are described in section 5.6 and 5.7.

In addition, a central part of the project was to disseminate the project results to the solar community, which was successfully done through presentations at expert meetings, conference participation and hosting of workshops. The dissemination activities are described in detail in section 5.8.

The project succeeded in realising its objectives, and the project results can be used by the solar industry. The international IEA Task 16 project has been prolonged, and it will finish in 2023. DMI and DTU will together participate in the Task as Danish participants, approximately on the same level as in this EUDP project.

5.1 Measurement of solar radiation in solar fields

To analyse the non-uniform irradiance distribution within collector array configurations and validate simulation models, high-precision measurement data of the irradiance distribution are necessary. The existence of such data sets did not exists prior to the project hence an experimental setup was created to emulate the irradiance conditions within a collector array.

The experimental setup was created with two rows of three collectors, thus the center rear collector experienced approximately the same irradiance conditions as any non-perimeter collector in a collector array. The irradiance distribution in the experimental array was then measured using ten high-precision pyranometers as shown in Figure 1.The setup was located on an even grass field on the campus of the Technical University of Denmark (DTU) in Kgs. Lyngby near Copenhagen (latitude 55.793°N, longitude 12.524°E, elevation 36 m).

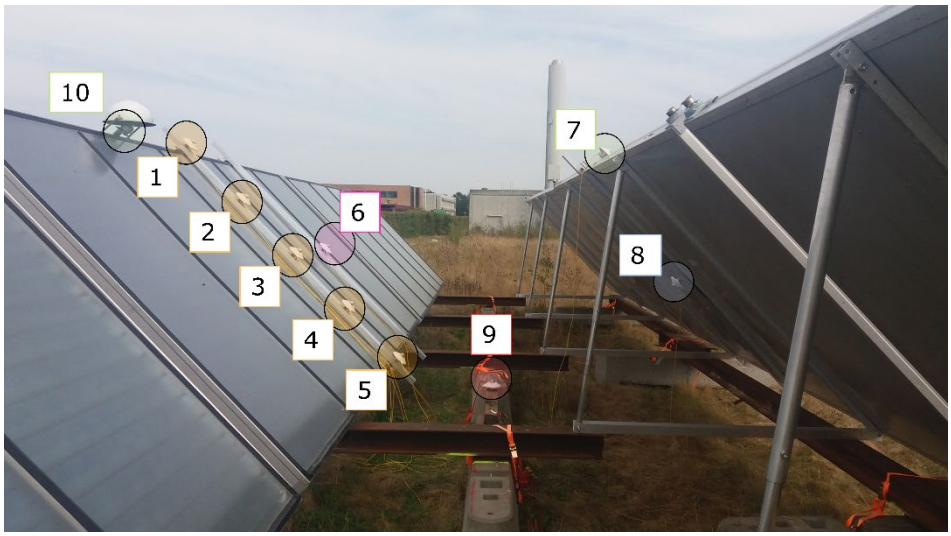

Figure 1: Experimental setup consisting of six flat-plate solar collectors and ten pyranometers (numbered).

Each of the six collectors was propped up with two adjustable aluminium poles, which made it possible to adjust the collector tilts. The second row of collectors was placed on I-beams, along which the collectors could slide allowing for the row spacing to be changed. The solar collectors were Sunmark flat-plate collectors which are used for large-scale solar thermal plants. The collectors were kept south-oriented during the entire measurement period. The backside of the collectors was unpolished aluminium with an assumed reflectance coefficient of 0.8. A reflectance coefficient of 0.2 was assumed for all ground segments due the lack of measurement.

In-plane irradiance was measured by pyranometers 1-7. Pyranometers 1-5 were used to measure the irradiance distribution along the collector height and therefore positioned with an even spacing along the center of the rear middle collector. Pyranometer 6 was offset to the side of 1-5 and repositioned during the experimental period for comparison purposes. Similarly to pyranometer 1, pyranometer 7 was placed on the collector in the front row. Pyranometer 8 was placed in the center of the backside of the front center collector. Pyranometer 9 was placed between the two collector rows horizontally. Pyranometer 10 was offset from pyranometer 1 and shaded by a half-dome covering the pyranometer's view to the sky. This was to investigate the reflected radiation from the ground and backside of the front collector row. Since all pyranometers, except for 9, were mounted in the collector plane, they changed tilt according to the adjusted tilt of the collectors. All sensors are Kipp & Zonen (K&Z) CMP11 instruments.

Experiments were conducted between August 2018 and May 2020. Measurements were made for two row spacings (3.5 m and 6 m) and three tilts (30°, 37.5°, and 45°), leading to six collector array configurations (CC) as shown in Table 1. All-sky conditions were used to obtain the validation data set for each setup, only discarding data which did not meet the filtering criteria and where instrument maintenance took place. The requirement to have no shading lead to the exclusion of most of the data from the winter periods.

Table 1: Investigated collector array configurations and valid data.

CC #	Row spacing	Tilt	Time period
1	3.5 m	45.0	Aug. 2018
2	3.5 m	37.5	Mar. – May. 2019
3	3.5 m	30.0	Aug. – Sep. 2019
4	6.0 m	45.0	Jul. 2019
5	6.0 m	37.5	May. – Jul. 2019
6	6.0 m	35.0	Mar. – May. 2020

Figure 2 illustrates typical results of the diffuse radiation distribution in collector arrays. Boxplots of five sensors within the array for configuration CC#1 and the diffuse horizontal irradiance at the DTU Climate Station are shown. Diffuse irradiance values on the ground, Du(P9), were calculated as the difference of global horizontal minus direct horizontal irradiance, accounting for direct radiation shading. Measurements on the top of the collector within the row, Dc(P1), and the front row, Dc(P7), are highly correlated (tau = 0.998 for CC #1, between 0.996 and 0.999 for other setups). Mean values for Dc(P7) are slightly higher be-cause of higher reflections (+2.3% for CC #1, between +1.8% and +4.0% for other setups). Dh lies in a similar range as Dc(P1) (+1.6% for CC #1, between -7.5% and +6.7% for other setups). The obstructed sky view of sensor P1 compared to Dh decreases the diffuse irradiance for isotropic conditions, but for anisotropic conditions the irradiance can be higher due the sensor being tilted. Du(P9) is aligned horizontally, however, it is substantially lower than Dh as the sensor does not see the whole hemisphere (-43.8% for CC #1, between -49.6% and -45.6% for other setups). Diffuse irradiance on the backside of the collector, Dc(P8), was 37.8 W/m2 on average for CC #1 and between 16.4 W/m2 and 53.3 W/m2 for the other setups. Dc(P10) had one-digit mean values close to zero (4.0 W/m2 for CC #1, between 1.9 W/m2 and 5.1 W/m2 for other setups). Note that the reported values give some indication of irradiance differences in various spots in a collector array, but should not be over interpreted, as the radiation experiments were conducted during different times of the year and only data fulfilling the filtering criteria were used. The validity of the model for 3D effects on the collector plane, i.e. irradiance differences in the east-west direction, was not the focus of the radiation experiments, although various placements of sensor P6 along the collector height next to sensors P1 to P5 showed that there was no significant difference between these measurements.

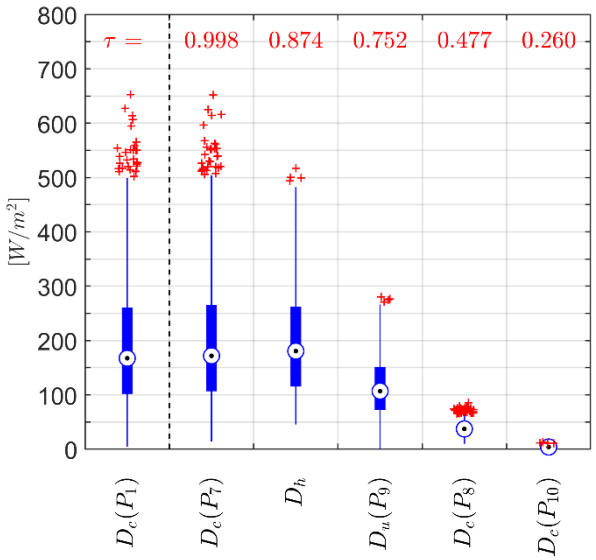

Figure 2: Box plot of diffuse irradiance at different spots in the collector arrayfor configuration CC #1. Red markers are outliers, τ is the Pearson correlationcoefficient with respect to Dc(P1).

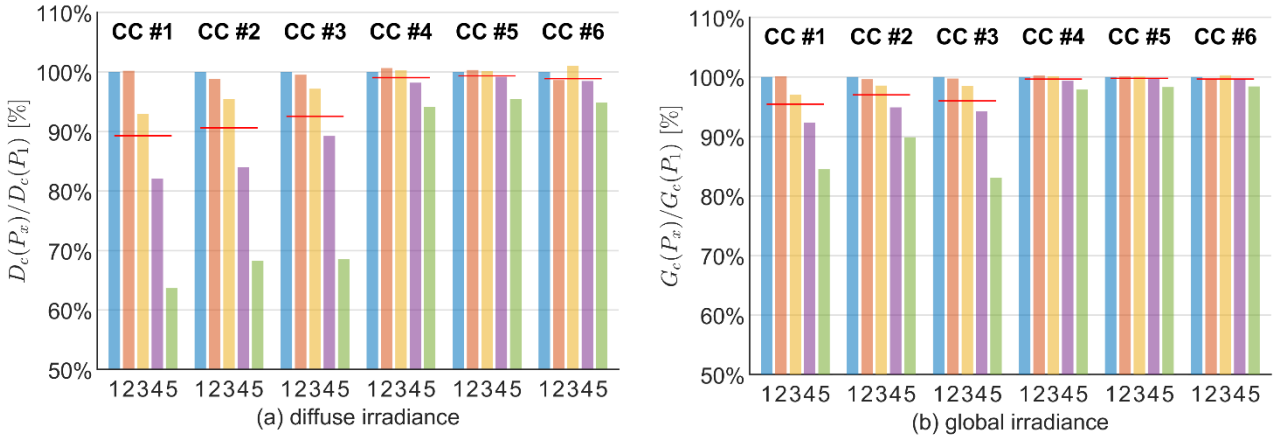

Figure 3: Irradiance distribution for (a) diffuse tilted irradiance and (b) globaltilted irradiance along the collector height relative to the top sensor (=100%). Numbers 1 to 5 refer to sensors P1 to P5. Red lines indicate averages among the five sensors.

For conditions without internal and external shading as usedfor the model validation, direct irradiance is constant alongthe collector height, but the diffuse irradiance varies from sen-sorsP1toP5as does the global tilted irradiance. Figure 3 shows the diffuse and global irradiance for all sensors normal-ized to P1(top sensor) (=100%) for all configurations. For the narrow row spacing (CC #1-3), the diffuse irradiance reduction is substantial, dropping as low as 63.7% for sensor P5 in CC #1, whereas for the wide row spacing (CC #4-6) the effectis marginal. Note that the diffuse irradiance levels for sensor P1 and P2 are very similar for all configurations. This is an indication of the obstructed horizon towards south, which makes sensors P1 and P2 receive essentially the same irradiance from the sky. Also note that P3 measures higher diffuse irradiance levels than P1 for CC #4-6. This atypical behavior can occur due to increased reflections which overcom-pensate for the reduced sky view. The reduction of global irradiance is less extreme, as all sensors receive the same direct irradiance. The global irradiancereduction is in tendency similar to the diffuse irradiance reduc-tion, but exposes some differences as the diffuse shares of the global irradiance vary among the setups.

A more detailed analysis of the diffuse irradiance reduction is shown in Figure 4, which displays the measured diffuse irradiance by sensors P2-P4 vs. the top sensor P1 for four configurations. The figure shows that the diffuse irradiance towards the bottom is not only lower, but that the scattering significantly increases.

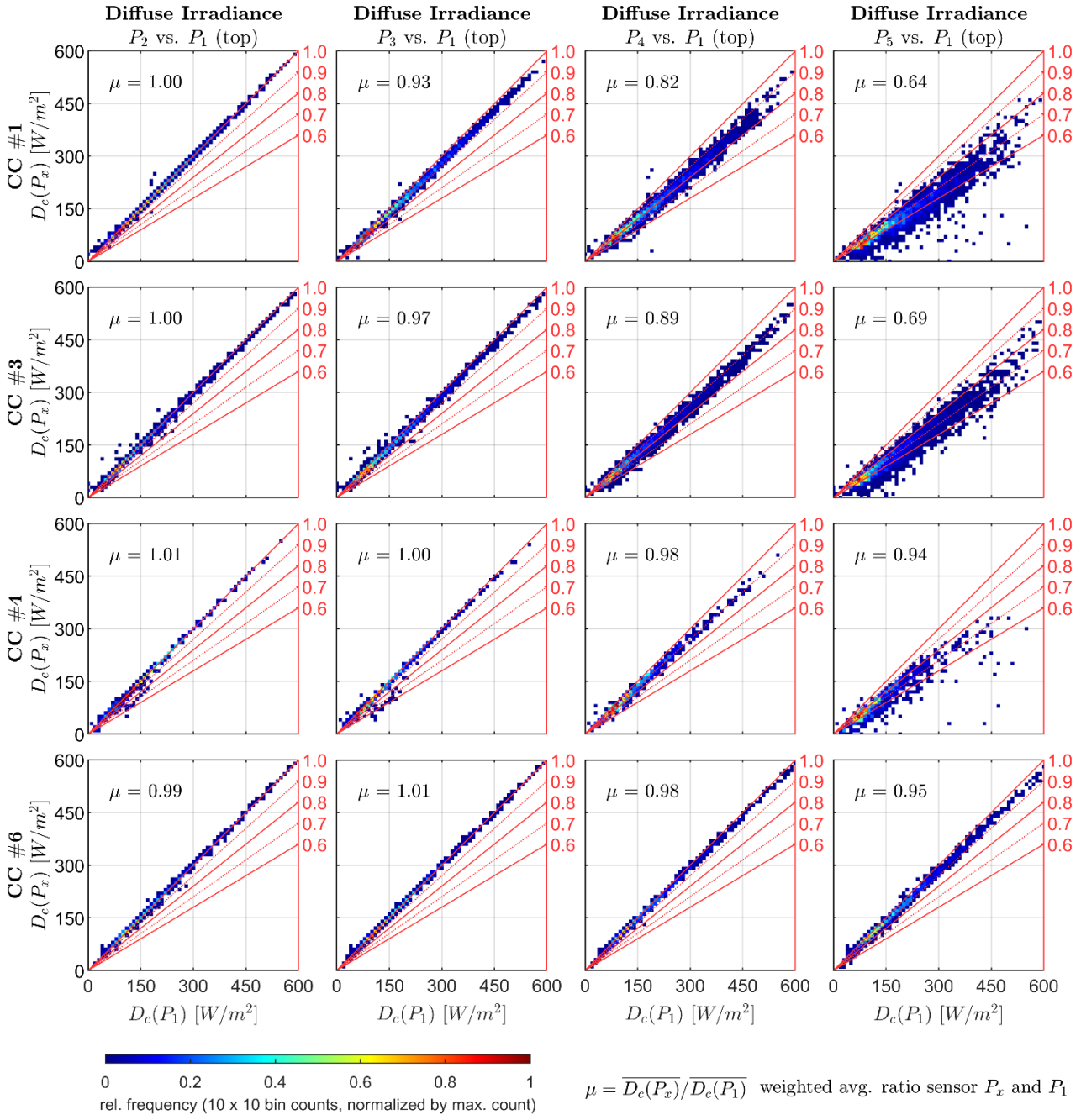

Figure 4:Measured diffuse irradiance on top and along the collector height for four configurations.

5.2 Modelling of solar radiation in solar fields

Practically all available solar radiation models assume the distribution of the diffuse irradiance on solar collector fields to be uniform, which clearly was demonstrated not to be true from the measurement analysis in the previous section. Such simplifications can results in significant errors when modelling the output of solar plants and forecasting their outputs. This leads to solar plants being incorrectly designed, hence to greater costs of renewable energy and a slower green transition. In this project we aimed to solve this issued by developing a new solar radiation transposition model Hay-C(Hay-and-Davies transposition model for collector arrays) which accounts for the unequal irradiance distribution by calculating the direct and diffuse irradiance for multiple segments along the collector height (see Figure 5). The number of segments m can be chosen according to the needed precision and resolution. If there are radiation sensors mounted in the same plane as the collector, the model additionally predicts the direct and diffuse irradiance on the sensors. The position of the sensors can be anywhere along the collector height or above the collector as well as with an offset perpendicular to the collector plane.

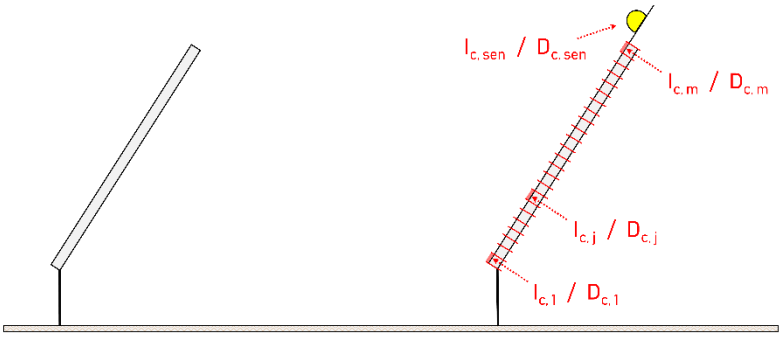

Figure 5: Segment-wise irradiance calculation.

The model can be applied both in the forward direction and inverse direction, depending on the purpose and available data. The forward direction (see Figure 6) is the typical collector array design case, where global horizontal irradiance Gh is known. First, the Erbs separation model is deployed to calculate the direct and diffuse irradiance components, Ih and Dh. The Hay-C model is then used to predict the direct and diffuse irradiance on each segment along the collector height,Ic,1...m and c,1...m, respectively. Calculating the average irradiance of all segments yields the direct and diffuse tilted irradiance, Ic,avg and Dc,avg, and their sum equals the global tilted irradiance Gc,avg. If either the direct irradiance (In or Ih) or diffuse horizontal irradiance Dh is also available, the separation model step can be skipped.

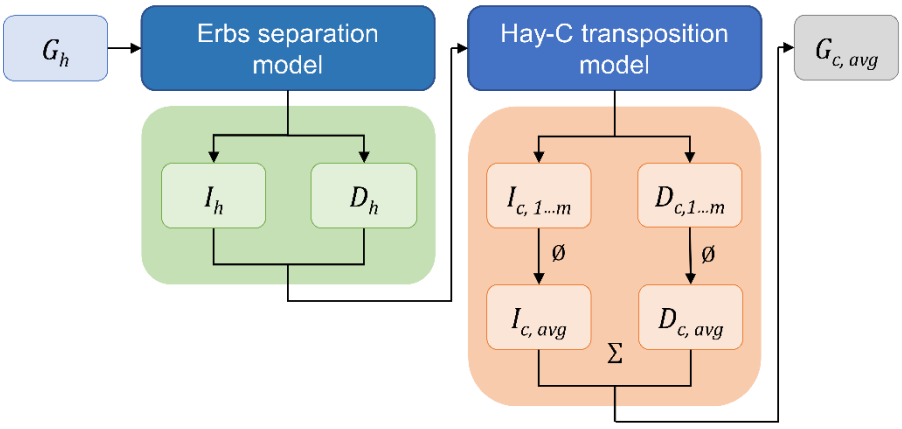

Figure 6: Calculation flow chart ofHay-Cmodel - forward direction..

For the model validation, data selection and collector array parameter setting was done as described in detail in (Tschopp, 2020). The number of collector segments was m=500, ground segments p=20 and backside segments q=20. Relative Mean Bias Error (%MBE) and relative Root Mean Square Error (%RMSE) were used as error metrics.

Two different cases were assessed for the forward direction, where the model tends to underestimate the global tilted irradiance at the top, Gc(P1). In the first case (A), the Erbs model over-estimates the direct horizontal irradiance and underestimates the diffuse horizontal irradiance and transposes this pattern to the tilted surface. In the second case (B), the diffuse tilted irradiance at the top is also underestimated, but to a lesser degree. For the inverse direction, two cases (C) and (D) were investigated, where the model overestimated the global horizontal irradiance with a bias similar in magnitude to the forward direction, but opposite in sign. The inverse direction shows reasonable accuracy, also for the split of the global irradiance in its direct and diffuse parts. Forward and in-verse direction behave the opposite way, which is an interesting modeling feature. For cases (A) and (C), which are suboptimal measurement setups compared to cases (B) and (D) as the direct radiation is not measured, modeling errors compensate. Surprisingly, this can result in a lower bias than for cases (B)and (D), although %RMSE are higher as is to be expected.

The accuracy of the model prediction for sensors P2 to P5 is shown in Figure 7 for all configurations, case (D). The model follows the distinct shape of the diffuse irradiance distribution along the collector height. The moleled irradiance for P2 is close to P1 as it is for the measurement, accounting for the obstructed horizon towards south. For the wide row spacing, CC #3-6, the model predicts the atypical behavior of slightly higher irradiance values for P3 than P1 due to increased reflections which overcompensate for the reduced sky view. The prediction accuracy for the sensors closer to the top sensor is significantly higher than for sensor P5, where the model over-estimates the diffuse irradiance substantially for the narrow row spacings CC #1-3. However, the diffuse irradiance prediction for the narrow row spacings is remarkably better than assuming the diffuse irradiance to be constant along the collector height which is the case for traditional transposition models.

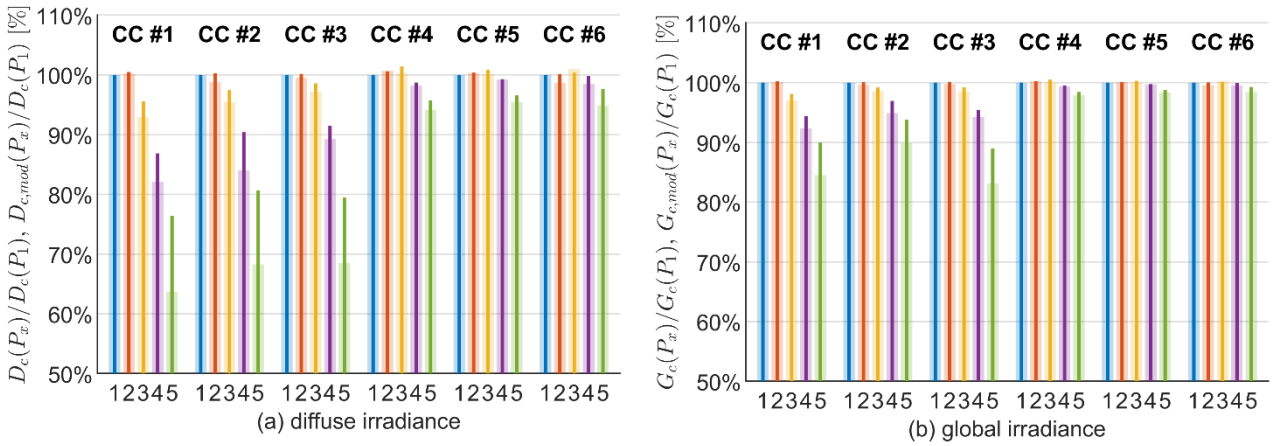

Figure 7: Modeled and measured comparison along the collector height for all configurations, Case (D). Distributions for (a) diffuse irradiance and (b) global irradiance are relative to the top sensor (=100%). Numbers 1 to 5 refer tosensors P1 to P5.

To demonstrate the importance of accurately modelling the non-uniformity of diffuse irradiance within solar fields, a case study has been carried out where the monthly energy production was calculated for a hypothetical solar collector and photovoltaic field. The two systems have been simulated for two different row spaces (3 and 6 m) and two different tilts (30° and 45°). The row spaces and tilts have been chosen to cover the range of possible configurations. Both the solar collector and photovoltaic panel were modelled with the same dimensions as the solar collector used for the measurement campaign in the previous section.

Furthermore, the solar collector was simulated for two different mean fluid temperatures, 50 and 70 °C, since this parameter has a large effect in terms of the thermal power output. The solar collector field was modelled as described in (Furbo, 2018) and was assumed to have the same collector parameters ($\eta_0 = 80.2\%$, $a_1 = 2.23 \frac{W}{m^2 K}$, and $a_2 = 0.01 \frac{W}{m^2 K^2}$). These parameters are representative of typical solar collectors seen in the large-scale solar collector fields in Denmark.

The simulation results for the solar collector field are shown in Figure 1. Each subplot represents a different configuration, i.e. row spacing and tilt, as labelled in the top right corner. The monthly heat production is calculated using the Hay-Davies model, representative of the current modelling approach in industry, and using the newly developed HayC model, which takes into account the reduction of diffuse irradiance due to irradiance masking by the collector row in front.

In Figure 8, it can be seen that there is a large difference between the HayC and the classical Hay & Davis modelling approach for the short row space (3 m). For the long row space (6 m) the difference in monthly energy production is small, where the classical approach clearly overestimated the energy production, which was also seen in the experiments in Section 4.1.1.

For both the short and long row space, the diffuse irradiance masking plays a smaller role for the lower tilt angle. This can be explained by the fact that the view angle to the sky is increased for the lower tilts. The heat production was significantly lower for the higher mean temperature investigated, due to greater heat losses. However, there was no noticeable difference with respect to mean temperature of the two radiation models.

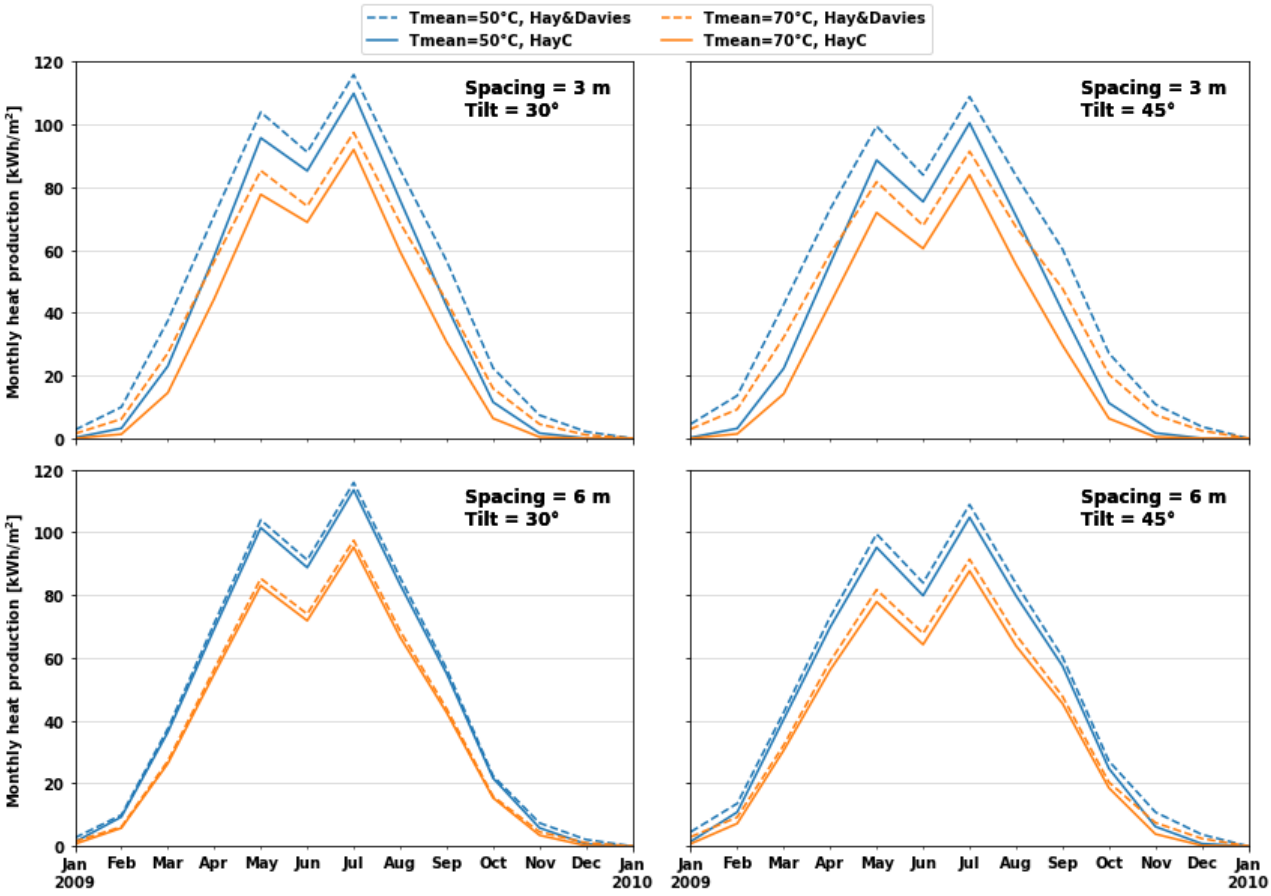

Figure 8: Comparison of monthly solar heat production using the original Hay-Davies model and the new developed HayC for different row spaces, tilt angles and mean solar collector fluid temperature.

Similarly, the impact on the monthly performance of photovoltaic (PV) panels in large-scale solar fields was investigated. In order to focus on the effects of the diffuse irradiance masking, a simplified approach was used for modelling the PV power output. Generic values for commonly installed mono-crystalline PV panels were chosen for the PV simulations. The power output for each timestamp was calculated as:

$$\frac{P_{pv}}{A} = G \cdot \eta_{mp,STC} \cdot K_\theta \cdot \left(1 - \alpha_P \cdot (T_{cell} - 25°\mathrm{C})\right) \qquad \text{Equation 1}$$

where G is the global tilted irradiance, $\eta_{mp,STC}$ is the efficiency at maximum power point under standard test conditions (assumed to be 19%), K_θ is the incidence angle modifier, α_P is the temperature dependent coefficient of power (assumed to be 0.4%), and T_{cell} is the cell temperature.

The reduction of the effective irradiance due to incidence angle losses was modelled according to the ASHRAE method, using an incidence angle coefficient of 0.06. It should also be noted that the last term in Equation 1, takes into account the reduced efficiency with increasing temperatures. The cell temperature is modelled as:

$$T_{cell} = T_{amb} + \frac{\mathrm{NOCT} - 20°\mathrm{C}}{800\,\frac{\mathrm{W}}{\mathrm{m}^2}}\,G \qquad \text{Equation 2}$$

Where T_{amb} is the ambient temperature, NOCT is the Nominal Operating Cell Temperature (assumed to be $45°\mathrm{C}$) and G is the global tilted irradiance.

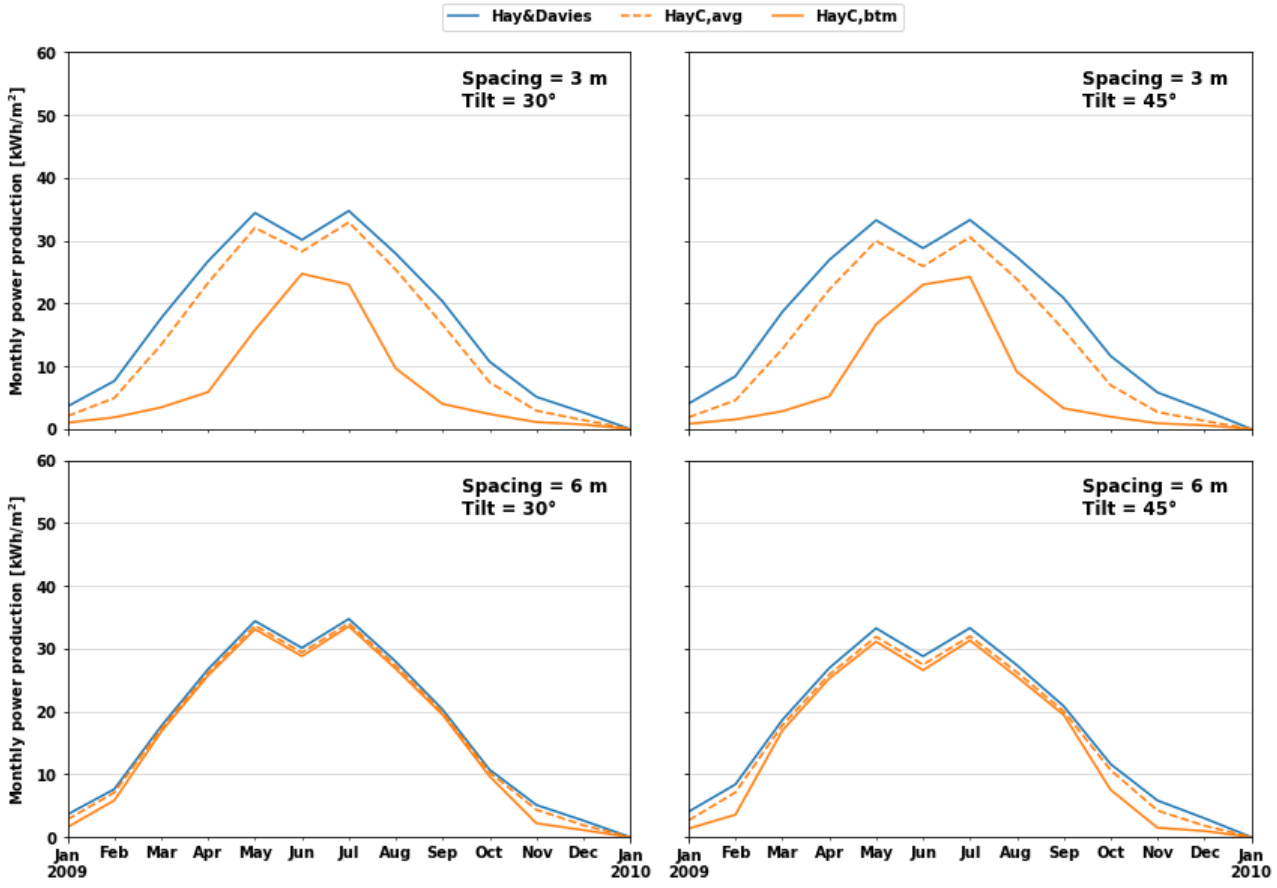

Figure 9: Comparison of monthly PV electricity production using the original Hay-Davies model and the new developed HayC for different row spaces and tilt angels.

The results of the PV simulations are shown in Figure 9, for the classical Hay & Davis modelling approach and for the average and bottom irradiance calculated by the HayC model. First, it is important to note that the output of a solar collector is independent of the distribution of irradiance, and is only affected by the average irradiance on the surface. PV panels, on the other hand, work in a very different way and experience mismatch losses. The mismatch loss depends on the layout of the PV cells, the layout of diodes and the distribution of irradiance. In Figure 9 the HayC,avg curve corresponds to an ideal case where the irradiance is completely uniform. The HayC,btm curve is the result of using the irradiance at the bottom of the collector, which is the lowest irradiance on the surface and would be the effective irradiance for a PV panel without any bypass diodes. The results for an actual PV panel with a finite number of bypass diodes would then be between these two curves.

The monthly PV production shows similar trends in that the difference between the classical modelling approach and the HayC model is greater for the short row space and the steep tilt angle. Again, for the long row space and the low tilt angle, the difference is very small and the classical modelling approach is sufficient. However, for both tilt angles for the short row space, using the classical approach results in even higher overestimations of the power production than for the solar collector scenario. This is especially prevalent if one considers the HayC,btm curve (corresponding to portrait PV panels or panels with no bypass diodes) where the classical approach is significant higher and the mismatch losses (difference between HayC,avg and HayC,btm) represents a significant share.

It has been clearly demonstrated that the diffuse irradiance masking is something that needs to be considered, especially for short row spaces and high tilts. The effect of this was found to be more extreme for PV panels due to the mismatch losses.

5.3 Quality control of solar radiation time series

It is virtually impossible to make continuous irradiance measurements without occasionally missing data and some form of erroneously data. While data providers often conduct a basic quality check, users of irradiance data are urged to conduct their own quality assessment. However, there exists numerous methods for this, but there is no commonly agreed upon methodology within the scientific community and hence each user often ends up with his or her own method of quality assessing data and treating questionable data.

Developing a standardized method for quality check of solar radiation data was the project's main contribution to subtask 2, which focused on best practices for pre-processing and quality control of solar radiation measurements.

Together with partners of the IEA Task 16 project the guide "Recommendations on good practices for the pre-processing, quality control of solar radiation measurements and example of validation tools" was developed. Example quality check steps are shown in Figure 10 and Figure 11.

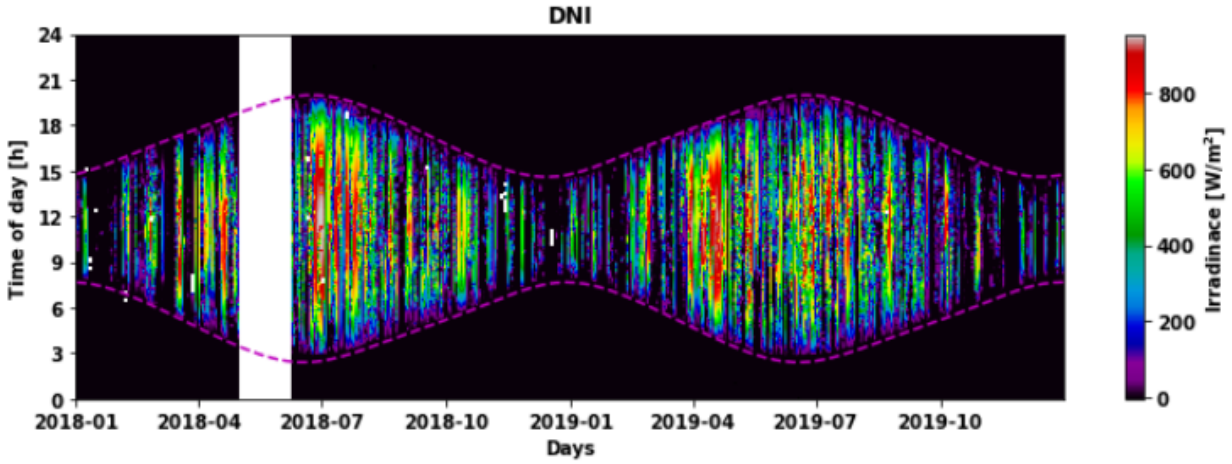

Figure 10: Two-dimensional visualization method of solar radiation data, where the x-axis corresponds to the day, the y-axis corresponds to the time of day, and the pixel color corresponds to the measurement value.

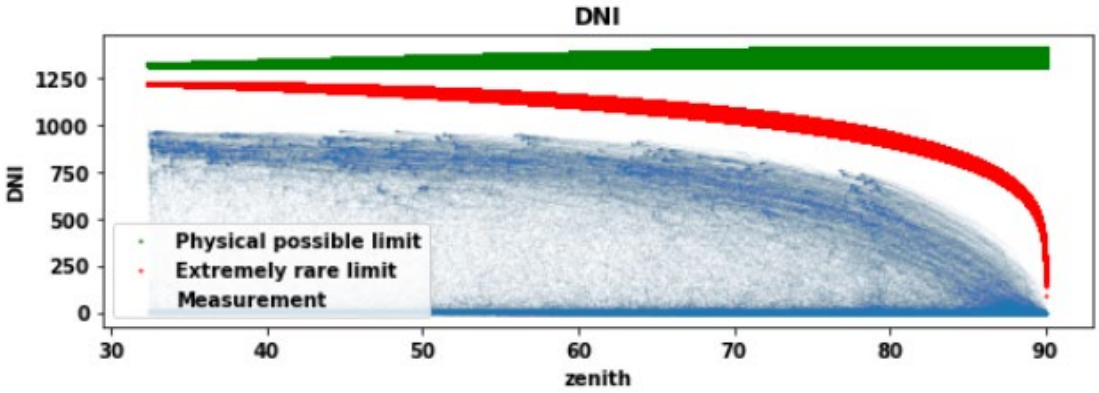

Figure 11: Example of the limit check step part of the quality-check.

5.4 Analyses of diffuse radiation measurements

Solar radiation measurements from the climate station of the Technical University of Denmark were analyzed in order to elucidate from which parts of the sky the diffuse radiation come. The climate station with 16 domes with opening areas corresponding to 1/8 and 1/16 part of the sky mounted over pyranometers and one dome is shown in Figure 12. The openings of the domes are facing the different parts of the sky.

Figure 12: The climate station at the Technical University of Denmark.

The investigations shows that the diffuse radiation from the sky is much higher from the sky close to the Sun disc than from the other parts of the sky under sunny conditions. Further, under cloudy conditions the diffuse radiation can be considered as isotropic, that is the solar radiation is coming uniformly from all parts of the sky.

5.5 Long-term inter-annual variability

DMI has lead the activity on this topic among the international partners. The effect of long-term inter-annual variability on the solar resource has been investigated in detail. It can be divided into 5 categories:

1. Inter-annual variability due to general weather changes from year to year.
2. Inter-annual variability due to global scale volcanic eruptions.
3. Long-term changes caused by other natural forcings than volcanic eruptions.
4. Long-term changes in atmospheric aerosols or clouds due to pollution.
5. Long-term changes in aerosols or clouds due to increased greenhouse gas concentrations.

In the following paragraphs the conclusions about each of these categories will be detailed. First some basic definitions are needed. The total annual solar yield of a particular solar technology can be assessed from the solar irradiance components. These components are the Direct Normal Irradiance (DNI), the Diffuse Horizontal Irradiance (DfHI), and the Reflected Horizontal Irradiance (RHI). Here the DNI is considered on a surface that always is directed at the sun, DfHI is the downward diffuse irradiance on a horizontal surface, and RHI is the upwards reflected diffuse irradiance on a horizontal surface. On tilted surfaces of solar heating or PV panels these components can be combined into Global (total) Titled Irradiances (GTI). For bifacial panels GTI can further be split into front and rear component as GTI_{front} and GTI_{rear}. Measured DNI includes DfHI within a certain angular range around the sun – typically within a half-angle of 2.5°. For concentrating solar technologies the utilized DNI resource will differ from the measured resource if they can only use a smaller (or large) half-angle than 2.5°. As described in section 5.2 other factors than the potentially available solar resource must be estimated to assess the total solar yield. Furthermore, the available solar irradiance must be considered in sufficiently high temporal resolution. For solar heating plants hourly resolution is needed, while minute resolution is needed for assessing yield of PV and concentrating solar plants.

The ***interannual variability due to general weather changes*** in clouds and aerosols from year to year affect the various irradiance components differently. Generally, DNI is more variable than GTI. For this reason, Design and Test Reference Years (DRYs/TRYs) or Typical Meteorological Years (TMYs) cannot be made optimally for all solar technologies. This is also why the annual yield, rather than the potentially available GTI or DNI, should be considered for specific technologies when assessing the variability. To concisely summarise the annual yield and variability two numbers are used: P50 and P90. Here P50 is the median value of the annual yield while P90 is the estimated probability of exceedance in 90% of all years, i.e. a year which yield statistically is exceeded in 90% of the years. In other words a bad year. Statistically, it is not possible to assess what a minimum yield year would be, and to reasonably estimate a P99 year it is necessary to base it on 100 years of irradiance data. The concept of using P50 and P90 is based on the premise that the annual fluctuations are stochastic and can be prescribed based on historical data. At least 10 years and preferably 30 years of historical data is needed. Empirical distributions or mathematical distributions, e.g. Gaussian or Weibull distributions, can be fitted to the historical data, and these then provide P50 and P90. In Figure 13 a frequency distribution of 43 years of DNI measurements from Phoenix, Arizona, is shown (Vignola et al. 2013) as an example together with a fitted mathematical distribution. In this case, a clear sky minus log-normal distribution is used with a clear sky DNI annual average value of 262 W/m^2, a mean value of -20 W/m^2, and a variance of 10 W/m^2. This distribution is a novelty and provides a better fit than for instance the Gaussian or Wakeby distributions used for the same data by Vignola et al. (2013). When fitting this distribution 4 outlier years with unusually low annual DNI values have been ignored. These years were affected by global scale volcanic eruptions, as will now be discussed. They provide an example of the shortcomings of basic statistical descriptions of inter-annual variability.

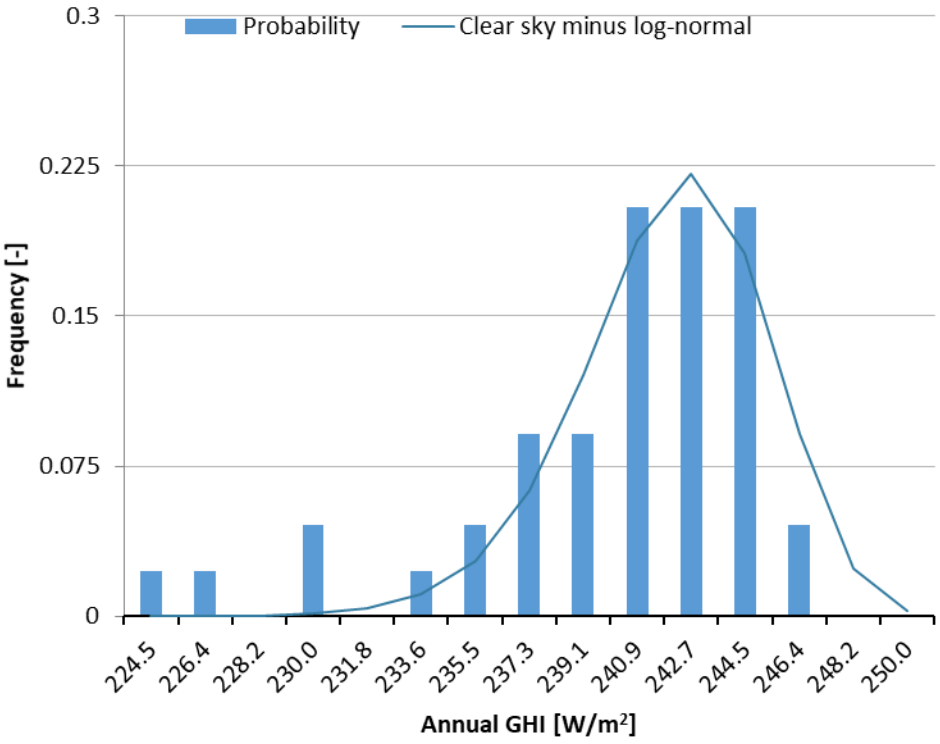

Figure 13: Frequency distribution of 43 years of annual average DNI measurements in Phoenix, Arizona, USA. The blue curve is a clear sky DNI minus log-normal distribution that is fitted to the data.

Inter-annual variability due to global scale volcanic eruptions is often forgotten due to the fact that a volcanic eruption at this scale has not occurred since the 1991 Pinatubo eruption. Thus, most ground-based and satellite-derived historical irradiance datasets do not include such events, and even the longest datasets only include so few cases that risk and magnitude distribution assessments cannot be made accurately.

Paleoclimatology studies can help. Sigl et al. (2015) analysed 2400 recent years of ice core data from Antarctica and Greenland for deposits of sulphuric acid. Following global scale volcanic eruptions small droplets of sulphuric acids are ejected high up into the stratosphere, where they can remain for several years before coming down again unlike mineral particles from the eruptions that quickly fall down. The stratospheric droplets are spread all around the world and some end up in the large ice sheets in the southern and northern arctic regions, where they over time are frozen into the glacial ice. From the deposit of sulphuric acid following the Pinatubo eruption and pyrheliometer measurements of the aerosol effects following this, the amount of deposited acid could be related to the aerosol optical depth (AOD) of this in the atmosphere. From this relation Sigl et al. could then assess aerosol optical depths linked to older deposits in the ice cores, and thereby their historical impact on the solar resource. Based on these data we have found that a global scale eruption with a stratospheric AOD of more than 0.1 on average occurs four times each century. Thus, planning of large-scale solar power plants, national and international energy planning for a future with high penetration of renewable energy must account for the occurrence of such eruptions. From the historical volcanic data, a Monte Carlo model that can simulate potential future eruptions has been made. Results from this are shown in Figure 14. Here each eruption is assumed to last for 50 days and have an e-folding time of 1 year (Crowley and Unterman 2013). To put these results in perspective a stratospheric AOD of 0.7 corresponds to a 50% reduction of the DNI resource. The reduction in the GTI resource is less, and the effect of the eruptions disappear after a few years, but clearly these events can be very disruptive.

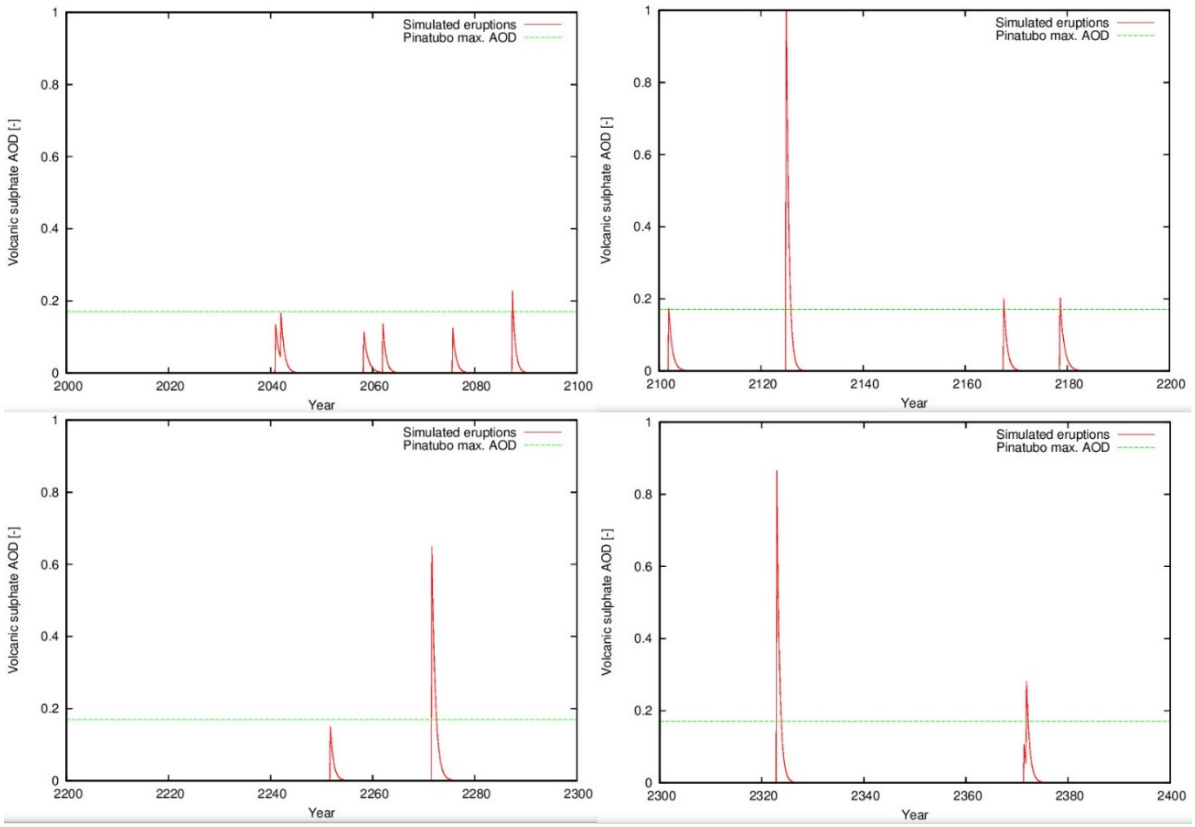

Figure 14: Simulated volcanic eruptions that cause stratospheric AODs or more than 0.1 over a period of four hundred years. The green line marks the highest magnitude of the 1991 Pinatubo eruption of a stratospheric AOD of 0.17.

Other natural forcings than volcanic eruptions have been considered to cause long-term changes in aerosols. In particular, changes in the solar activity and total solar irradiance has been suspected to affect the overall solar resource significantly. Recent studies based on 40 years of satellite data covering both very active and less active solar cycles, however, have shown that the Sun is a remarkably stable star (Coddington et al. 2016) varying only within 0.2% percent even over a 400 year period (Kopp et al. 2016).

Long-term changes in atmospheric aerosols or clouds due to pollution have been suggested to be a major influence on the solar resource. Thus, Wild (2012) has shown that periods with increasing and decreasing pollution in different regions of the world correspond to periods with decreasing and increasing solar irradiance at the surface. These periods are referred to as periods of “global brightening” and “global dimming”, respectively. The occurrence of these adds uncertainty to the usage of DRY/TRY/TMY yearly datasets or P50 and P90 values that are derived from historical irradiance data. If these are based on data from decades less or more polluted than the coming decades they will be misleading. Current atmospheric models used for climate scenarios still struggle with representing the effect that pollution has directly on the atmospheric aerosol forcing and indirectly via aerosol-cloud modification. Here polluting aerosols can both cause clouds to reflect more solar irradiance and affect the lifetime of these. In particularly these indirect effects are still a challenge to model accurately. Here more work is needed!

The impact of increased greenhouse gases on the long-term solar resource is also worth considering. If these shift the overall weather patterns, the cloud occurrence will also shift. If a region will get less rain in the future, the ground can dry out leading to a vicious cycle with the dryer ground decreases the potentially present cloud water, which again increases the solar irradiance drying the ground further. In our studies, and those from other countries, such effects have, however, not been identified to be of significance. To the extent that they are, they are less than the effect from aerosol pollution mentioned above.

5.6 Products for end-users

This part of the project has been particularly supported by the IEA SolarPACES programme, who have provided additional funds for international meetings. The objective in this activity is to concisely convey where solar radiation products can be found, and why and how to use them. There are several types of end users, who will need different products at different project stages. For this reason, we have organized the solar radiation products according to different use cases as shown in Table 2. For each of these categories product specifications and minimal requirements have been made.

Table 2: Tabular classification of solar radiation product end users and project stages.

	Category of Product / service	Project developers needs at different plant stages					Other users		
		(A) Pre-feasibility	(B) Feasibility and design	(C) Due Diligence Financing	(D) Plant Acceptance Tests	(E) Systems or Plant Operations	(F) Grid operators	(G) Policy makers	(H) Education / Outreach
1	GIS and maps	O				O	O	O	O
2	Consultancy services - measurements and stations		O	O	O	O		O	O
3	Modeled and satellite-derived datasets	O	O	O		O			O
4	TMY and MY90 series in a specific location	O	O	O				O	O
5	Variability	O	O	O				O	O
6	Local low level attenuation	O	O	O	O	O		O	O
7	Sunshape	O	O	O	O	O		O	O
8	Forecasting and nowcasting		O	O	O	O	O	O	O
9	Solar radiation sensors - Calibration and maintenance		O	O	O	O		O	O

5.7 Yearly thermal performances of Danish solar heating plants

Investigations of the measured yearly thermal performances of Danish solar heating plants were carried out. The measurements are carried out with conventional energy meters in the secondary loop of the solar collector fields with water as the heat transfer fluid. The solar radiations are typically measured with inexpensive pyranometers on the top of collectors inside the collector fields. The measurements are available on the website www.solvarmedata.dk (2020). Measurements for 69 solar heating plants in the period 2012-2019 are included in the investigation. The collector aperture areas of the solar heating plants are in the interval from 2970 m² to 70000 m², the collector tilts are in the interval from 30° to 45° and all of the collectors are facing south. The solar heating plants, which were installed in the period 1996-2018, are located in different zones of global radiation in Denmark, see Figure 15 and Table 3.

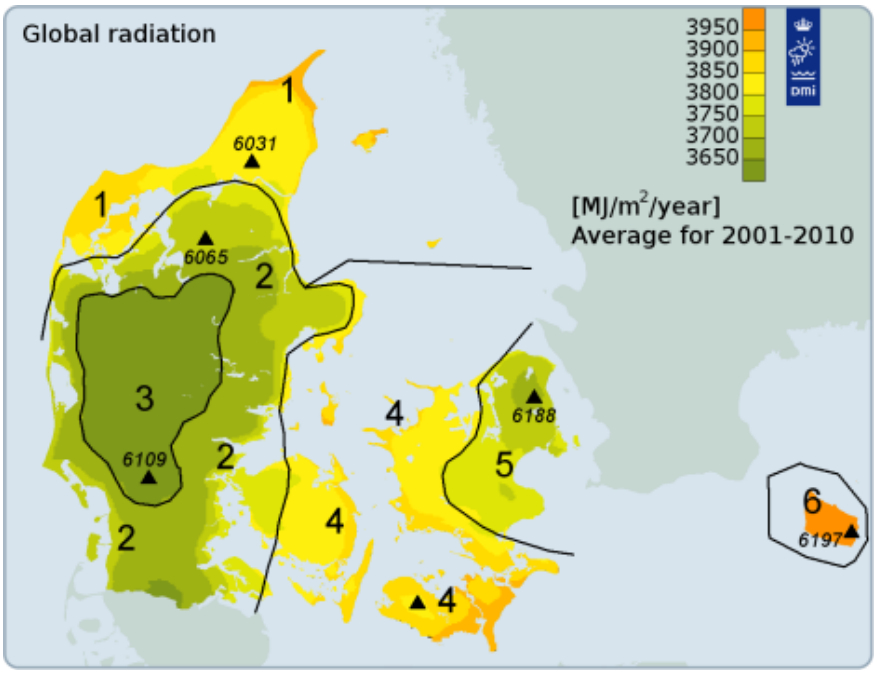

Figure 15: Solar radiation zones of Denmark.

Table 3: Location of solar heating plants in investigations.

Solar radiation zone	Number of solar heating plants
1	13
2	14
3	19
4	17
5	6
6	0
Total	69

The measured yearly thermal performances per aperture solar collector area for the solar heating plants as function of the measured solar radiation on the collectors for all years and all zones are shown in Figure 16.

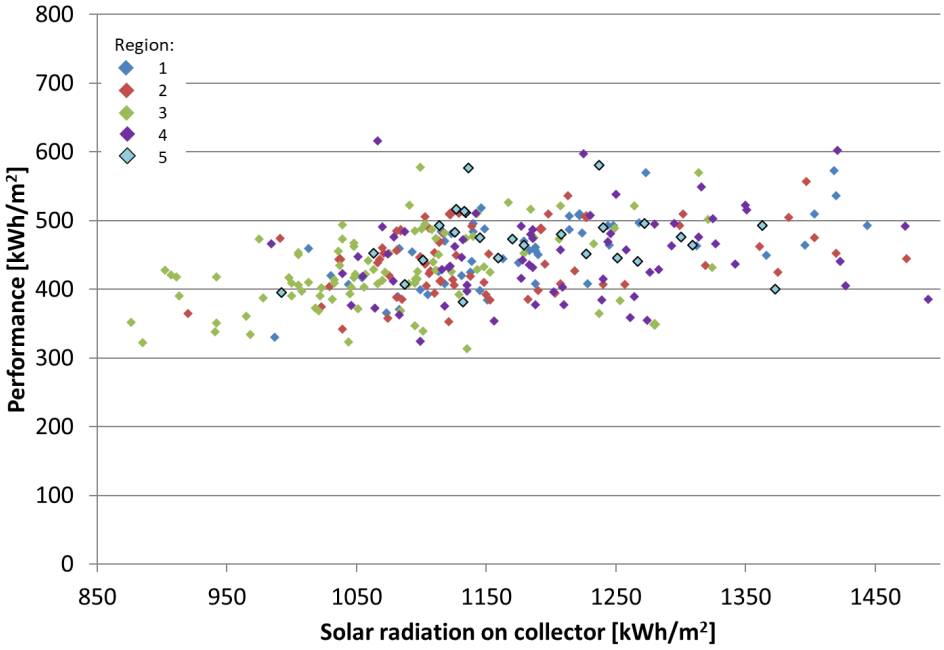

Figure 16. Yearly thermal performances as function of yearly solar radiation on solar collectors for all plants and years.

The measured yearly thermal performances of the solar heating plants per collector area ranged from 313 kWh/m² to 616 kWh/m² with yearly averages for all plants between 407 kWh/m² and 494 kWh/m². The measured yearly solar radiations on the solar collectors were in the interval 848 kWh/m² collector - 1491 kWh/m² collector with yearly averages for all plants between 1101 kWh/m² and 1246 kWh/m². The yearly utilizations of the solar radiation were in the interval 26% - 58%, with yearly averages for all plants between 36% and 42%. It is estimated, that the measured thermal performances and utilizations of the solar radiation for all the plants are satisfactory high.

There are many reasons for the differences in thermal performances between the different solar heating plants. First of all, different weather conditions from location to location and from year to year will influence the yearly thermal performance. It appear from Figure 25 that the yearly thermal performance is increasing for increasing yearly solar radiation. Further, there are different temperature levels in the different district heating systems. This will result in different temperature levels in the solar collector fields and therefore in different thermal performances. The lower the temperature level is, the higher the thermal performance.

Furthermore, the different solar collector types, the different designs of the solar collector fields, the different control strategies including the different flow rates and maybe the different uneven flow distributions in the solar collector fields will influence the thermal performance.

Yearly thermal performances of a solar collector field have been calculated for the six different Danish zones shown in Figure 15. The calculations have been done with the efficiency and incidence angle modifier of a typical marketed solar collector.

Calculations are carried out for each zone and each year with measured weather data from the period 2002-2010. An hourly value for the global radiation on horizontal is measured for every hour of the years. The method described by (Dragsted and Furbo, 2012) is used to calculate the hourly diffuse and direct radiation on horizontal.

Figure 17 and Figure 18 show the results for the nine years period 2002-2010. These include the measured yearly global radiation on horizontal, the calculated total yearly radiation on the collectors and the calculated yearly thermal performance of the collector field as a function of the mean solar collector fluid temperature

which is assumed constant during all operation periods for zone 1, see Figure 15. Further, the values for the design reference year for the zone (Wang, Scharling and Nielsen, 2012) are included in the figures. The performance ratio included in Figure 18 is defined as the ratio between the thermal performance of the solar collector field for the year in question and the thermal performance of the solar collector field for the reference year for the region.

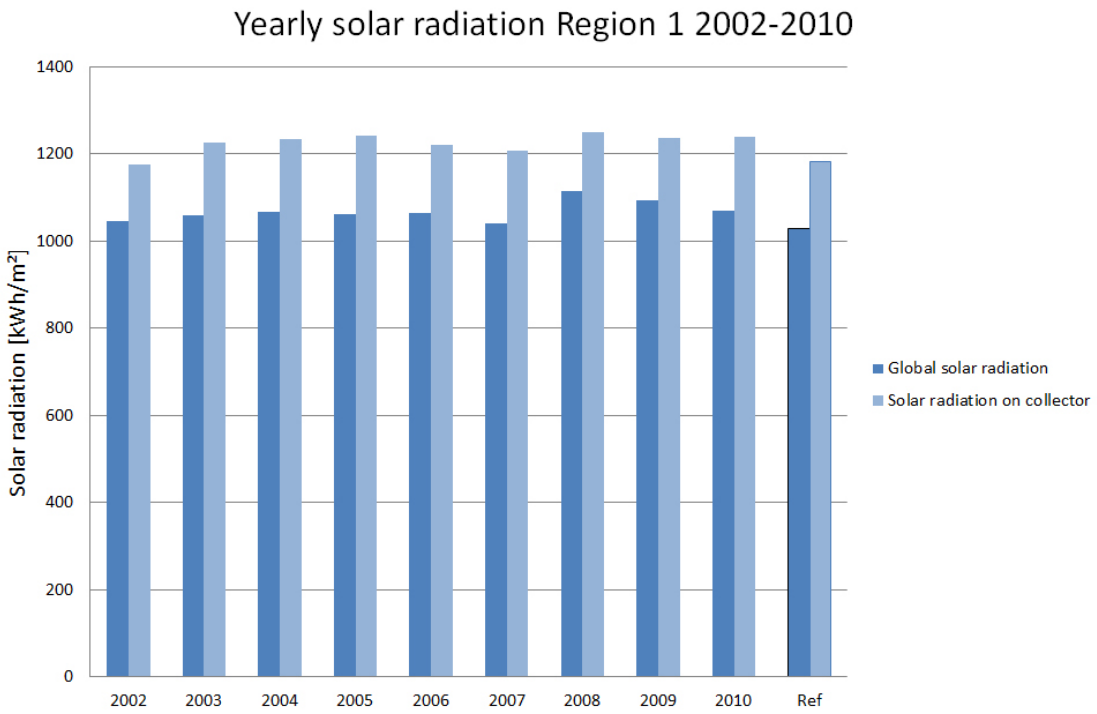

Figure 17: Measured yearly global radiation and calculated yearly solar radiation on collectors for zone 1.

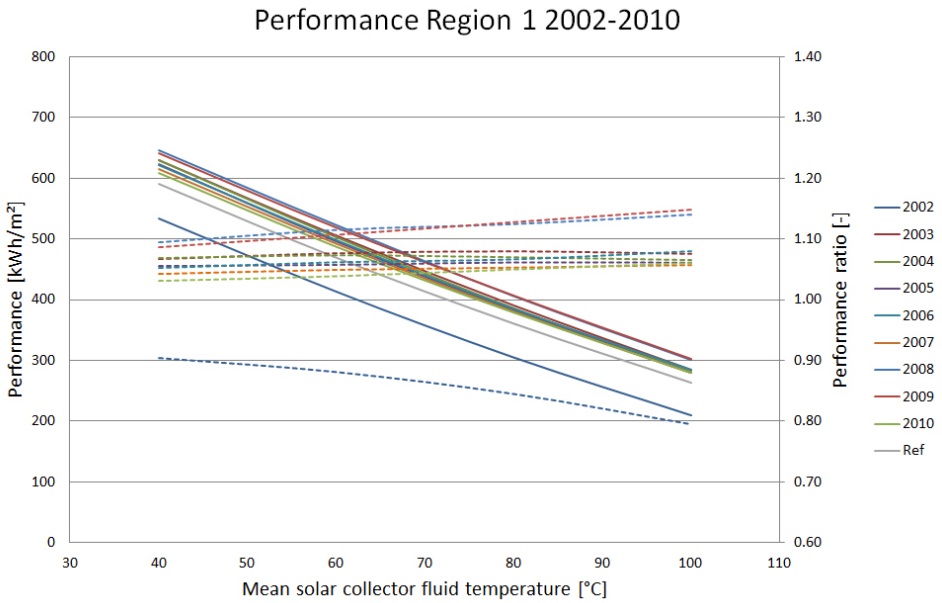

Figure 18: Calculated yearly thermal performance of a collector field for zone 1.

Figure 19 shows the highest and lowest yearly thermal performances for all six zones for all years as a function of the mean solar collector fluid temperature.

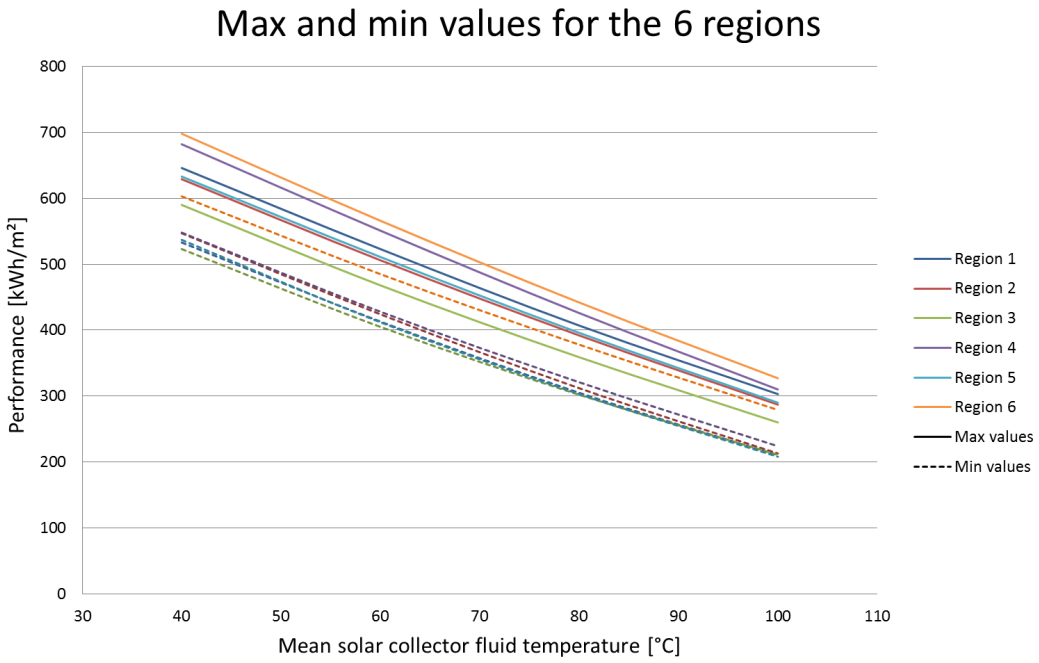

Figure 19: Calculated highest and lowest yearly thermal performance for the Danish zones as a function of the mean solar collector fluid temperature.

The measured yearly global radiations on horizontal for all years and all zones are in the interval 980 kWh/m² - 1150 kWh/m². The highest yearly global radiation is 17% higher than the lowest yearly global radiation. The highest yearly global radiation is measured in zone 6, Bornholm for 2005. The lowest yearly global radiation is measured in zone 3, the inner parts of Jutland for 2004.

Based on the hourly global radiation measurements, the hourly solar radiations on the collectors are calculated. Shadows from the row placed in front of the collectors are considered. The calculated yearly solar radiations on the collectors are in the interval 1077 kWh/m² - 1337 kWh/m². The highest yearly solar radiation on the collectors is 24% higher than the lowest yearly solar radiation on the collectors. Again, the highest yearly solar radiation on the collectors is for zone 6, Bornholm for 2005 and the lowest yearly solar radiation on the collectors is for zone 3, the inner parts of Jutland for 2004.

The yearly thermal performance is strongly influenced by the mean solar collector fluid temperature. For decreasing temperature, the yearly thermal performance is increasing and the percentage differences between the yearly thermal performances from year to year are decreasing.

The yearly thermal performances of the solar collectors typically are highest in region 6, Bornholm followed by zones 1 and 4, the northern part of Jutland and Funen & the western part of Zealand, zone 5, the eastern part of Zealand, zone 2, parts of Jutland close to the coastline and last zone 3, the inner parts of Jutland.

The highest and lowest yearly thermal performances for the solar collector field with a mean solar collector fluid temperature of 60°C are listed in Table 4 for the six zones.

Table 4: Calculated highest and lowest yearly thermal performances of solar collector field for the period 2002-2010 for six zones with a mean solar collector fluid temperature of 60°C.

Zone	Highest thermal performance, kWh/m² collector	Lowest thermal performance, kWh/m² collector	Ratio between highest and lowest yearly thermal performance, -
1	523	413	1.27
2	506	424	1.19
3	468	405	1.16
4	551	428	1.29
5	511	412	1.24
6	566	485	1.17

For a mean solar collector fluid temperature of 60°C the yearly thermal performance is in the interval 405 - 566 kWh/m² collector. The lowest thermal performance is calculated for 2004 for zone 3, the inner parts of Jutland. The highest calculated thermal performance is for 2005 for zone 6, Bornholm. The highest yearly thermal performance is 40% higher than the lowest yearly thermal performance.

The percentage differences between the highest and lowest yearly thermal performance of the collectors are lowest in zone 3, the inner parts of Jutland, followed by zone 6, Bornholm, zone 2, parts of Jutland close to the coastline, zone 5, the east-ern part of Zealand, zone 1, the northern part of Jutland, and last zone 4, Funen & the western part of Zealand.

The investigations showed that about half of the variations of the yearly thermal performances of the solar heating plants were caused by variations of the yearly solar radiation.

5.8 Dissemination

The project results were disseminated by participation in the following expert meetings of the IEA Task 16 project:

- Participation in expert meeting in March 2018 in Paris, France.
- Participation in expert meeting in September 2018 in Rapperswil, Switzerland.
- Participation in expert meeting in April 2019 in Utrecht, the Netherlands.
- Participation in expert meeting in November 2019 in Santiago, Chile.
- Participation in online expert meeting in March 2020.
- Participation in online expert meeting in September 2020.
- Participation in online expert meeting in November 2020.

Further, project results were disseminated by participation at the following conferences:

- Presentation on solar radiation at IEA SolarPACES Task V meeting on “Solar radiation products for end users” in October 2018 in Casablanca, Morocco.
- Organisation of the workshop: ”*IEA PVPS Task 16: Best practices for quality control procedures and gap filling methods*” at the International Conference Energy & Meteorology (ICEM) in June 2019 in Kgs. Lyngby, Denmark. Also, presentation of ”Gap filling of long-term solar radiation measurements in Denmark”.

- Keynote presentation on solar radiation modelling, uncertainty and quality control at EMS (European Meteorological Society) 2019 annual meeting in September 2019 in Kgs. Lyngby, Denmark.
- Presentation of developed solar radiation quality control procedures at The 30th International Photovoltaic Science and Engineering Conference (PVSEC-30, Korea) on November 11th, 2020.

Project results were also disseminated by publications of papers in scientific journals and reports:

- Blanc, P., Boilley, A., Gschwind, B., Jensen, A. R., Menard, L., Saint-Drenan, Y. (2020). Recommendations on good practices for the preprocessing, quality control of solar radiation measurements and example of validation tools. https://github.com/YvesMSaintDrenan/IEA_PVPS_T16_QC_pynb
- Furbo, S., Dragsted, J., Perers, B., Andersen, E., Bava, F., & Nielsen, K. P. (2018). Yearly thermal performances of solar heating plants in Denmark – Measured and calculated. Solar Energy, 159, 186–196. https://doi.org/10.1016/j.solener.2017.10.067
- Nielsen, K. P. (2019). 2001 - 2010 Danish Design Reference Year. Update and supplementary datasets. DMI Report 18-20. https://www.dmi.dk/fileadmin/Rapporter/2018/DMI_report_18-20.pdf
- Nielsen, K. P., & Gleeson, E. (2018). Using Shortwave Radiation to Evaluate the HARMONIE-AROME Weather Model. Atmosphere, 9(5). https://doi.org/10.3390/atmos9050163
- Rontu, L., Gleeson, E., Perez, D. M., Nielsen, K. P., & Toll, V. (2020). Sensitivity of radiative fluxes to aerosols in the ALADIN-HIRLAM numerical weather prediction system. Atmosphere, 11(2), 205. https://doi.org/10.3390/atmos11020205
- Sengupta, M., Habte, A., Gueymard, C. & Stoffel, T. (2017). Best Practices Handbook for the Collection and Use of Solar Resource Data for Solar Energy Applications: Second Edition. NREL. https://www.nrel.gov/docs/fy18osti/68886.pdf
- Tschopp, D., Jensen, A. R., Dragsted, J., Ohnewein, P., Furbo, S. (2020 in review). Measurement and modeling of diffuse irradiance masking on tilted planes for solar engineering applications. Submitted to Applied Energy.

Students following solar energy courses at the Technical University of Denmark have been informed about the project results.

Finally, detailed solar radiation measurements and measured climate data can be downloaded from the homepage: http://climatestationdata.byg.dtu.dk/.

6. Utilisation of project results

DMI and DTU will participate in the international IEA Task project until the end of the Task in 2023. The project results will form the basis for the continued work within the Task. The project results will not be utilized commercially, and no patents will be taken out.

The results are useful for energy planners and decision makers aiming to establish a sustainable energy system fully based on renewables.

The project has contributed to a PhD study, and the project results have been presented for students following courses at the Technical University of Denmark.

7. Project conclusion and perspective

The project resulted in a better understanding of the solar energy resource. Among other things, detailed solar radiation measurements with good quality were made available from the climate station of the Technical University of Denmark in Kgs. Lyngby, updated solar radiation data for the Danish Design Reference Year were worked out, recommendations on solar radiation measurements were prepared, a solar radiation model for large solar energy fields was developed, the weather's influence on the thermal performance of solar heating plants was elucidated and the inter-hourly and hourly spatio-temporal variability of the solar resource and the long-term inter-annual variability of solar radiation were elucidated.

Based on the project results better recommendations on energy systems with high degree of renewable energy penetration can be given to energy planners and decision makers. Further, the project results are valuable for the solar energy industry in connection with their efforts to develop, design and optimize their solar energy systems in the best possible way.

8. Appendices

Blanc, P., Boilley, A., Gschwind, B., Jensen, A. R., Menard, L., Saint-Drenan, Y. (2020). Recommendations on good practices for the preprocessing, quality control of solar radiation measurements and example of validation tools. https://github.com/YvesMSaintDrenan/IEA_PVPS_T16_QC_pynb

Coddington, O., Lean, J. L., Pilewskie, P., Snow, M., & Lindholm, D. (2016). A SOLAR IRRADIANCE CLIMATE DATA RECORD. Bulletin of the American Meteorological Society, 97(7), 1265–1282. https://doi.org/10.1175/BAMS-D-14-00265.1

Crowley, T.J., Unterman, M.B. (2013). Technical details concerning development of a 1200 yr proxy index for global volcanism. Earth System Science Data, 5 (1), 187.

Dragsted, J., & Furbo, S. (2012). Solar radiation and thermal performance of solar collectors for Denmark. Technical University of Denmark, Department of Civil Engineering. DTU Byg report R-275.

DTU Climate Station. Solar radiation measurements from DTU's climate station in Kgs. Lyngby can be downloaded from: http://climatestationdata.byg.dtu.dk/

Furbo, S., Dragsted, J., Perers, B., Andersen, E., Bava, F., & Nielsen, K. P. (2018). Yearly thermal performances of solar heating plants in Denmark – Measured and calculated. Solar Energy, 159, 186–196. https://doi.org/10.1016/j.solener.2017.10.067

IEA Task 16 homepage: https://iea-pvps.org/research-tasks/solar-resource-for-high-penetration-and-large-scale-applications/

Kopp, G., Krivova, N., Wu, C. J., Lean, J. (2016). The impact of the revised sunspot record on solar irradiance reconstructions, Solar Phys., doi:10.1007/s11207-016-0853-x.

Sengupta, M., Habte, A., Gueymard, C. & Stoffel, T. (2017). Best Practices Handbook for the Collection and Use of Solar Resource Data for Solar Energy Applications: Second Edition. NREL. https://www.nrel.gov/docs/fy18osti/68886.pdf

Nielsen, K. P. (2019). 2001 - 2010 Danish Design Reference Year. Update and supplementary datasets. DMI Report 18-20. https://www.dmi.dk/fileadmin/Rapporter/2018/DMI_report_18-20.pdf

Nielsen, K. P., & Gleeson, E. (2018). Using Shortwave Radiation to Evaluate the HARMONIE-AROME Weather Model. Atmosphere, 9(5). https://doi.org/10.3390/atmos9050163

Sigl, M., Winstrup, M., McConnell, J.R., Welten, K.C., Plunkett, G., Ludlow, F., Büntgen, U., Caffee, M., Chellman, N., Dahl-Jensen, D. and Fischer, H. (2015). Timing and climate forcing of volcanic eruptions for the past 2,500 years. Nature, 523 (7562), 543-549.

SolvarmeData.dk. (2020). Thermal performance of solar heating plants available at: www.solvarmedata.dk

Rontu, L., Gleeson, E., Perez, D. M., Nielsen, K. P., & Toll, V. (2020). Sensitivity of radiative fluxes to aerosols in the ALADIN-HIRLAM numerical weather prediction system. Atmosphere, 11(2), 205. https://doi.org/10.3390/atmos11020205

Tschopp, D., Jensen, A. R., Dragsted, J., Ohnewein, P., Furbo, S. (2020 in review). Measurement and modeling of diffuse irradiance masking on tilted planes for solar engineering applications. Submitted to Applied Energy.

Vignola, F.E., McMahan, A.C., Grover, C.N. (2013). Bankable Solar-Radiation Data sets, in: Solar Energy Forecasting and Resource Assessment. Elsevier, pp. 97–131. doi:10.1016/B978-0-12397177-7.00005-X

Wang, P. R., Scharling, M., & Nielsen, K. P. (2012). 2001-2010 Design Reference Year for Denmark. DMI, Technical Report 12-17, Copenhagen, Denmark. https://www.dmi.dk/fileadmin/Rapporter/TR/tr12-17.pdf

Wild, M. (2012). Enlightening global dimming and brightening. Bulletin of the American Meteorological Society, 93 (1), 27-37.